Published in final edited form as:
Angew Chem Int Ed Engl. 2013 July 29; 52(31): 8074–8078. doi:10.1002/anie.201301135.

Multi-Chromatic pH-Activatable ^{19}F-MRI Nanoprobes with Binary ON/OFF pH Transitions and Chemical Shift Barcodes**

Xiaonan Huang,
Department of Pharmacology, Harold C. Simmons Comprehensive Cancer Center, UT Southwestern Medical Center at Dallas, 5323 Harry Hines Blvds, Dallas.Texas 75390 (USA)

Gang Huang,
Department of Pharmacology, Harold C. Simmons Comprehensive Cancer Center, UT Southwestern Medical Center at Dallas, 5323 Harry Hines Blvds, Dallas.Texas 75390 (USA)

Shanrong Zhang,
Advance Imaging Research Center, UT Southwestern Medical Center at Dallas, 5323 Harry Hines Blvds, Dallas.Texas 75390 (USA)

Koji Sagiyama,
Advance Imaging Research Center, UT Southwestern Medical Center at Dallas, 5323 Harry Hines Blvds, Dallas.Texas 75390 (USA)

Osamu Togao,
Advance Imaging Research Center, UT Southwestern Medical Center at Dallas, 5323 Harry Hines Blvds, Dallas.Texas 75390 (USA)

Xinpeng Ma,
Department of Pharmacology, Harold C. Simmons Comprehensive Cancer Center, UT Southwestern Medical Center at Dallas, 5323 Harry Hines Blvds, Dallas.Texas 75390 (USA)

Yiguang Wang,
Department of Pharmacology, Harold C. Simmons Comprehensive Cancer Center, UT Southwestern Medical Center at Dallas, 5323 Harry Hines Blvds, Dallas.Texas 75390 (USA)

Yang Li,
Department of Pharmacology, Harold C. Simmons Comprehensive Cancer Center, UT Southwestern Medical Center at Dallas, 5323 Harry Hines Blvds, Dallas.Texas 75390 (USA)

Todd C. Soesbe,
Advance Imaging Research Center, UT Southwestern Medical Center at Dallas, 5323 Harry Hines Blvds, Dallas.Texas 75390 (USA)

Baran D. Sumer,
Department of Otolaryngology, UT Southwestern Medical Center at Dallas, 5323 Harry Hines Blvds, Dallas.Texas 75390 (USA)

Masaya Takahashi,
Advance Imaging Research Center, UT Southwestern Medical Center at Dallas, 5323 Harry Hines Blvds, Dallas.Texas 75390 (USA)

**This work is supported by the NIH (R01CA129011, R01EB013149). We acknowledge the assistance of the Southwestern Small Animal Imaging Resource, which is supported in part by NCI U24 CA126608, the Simmons Cancer Center through an NCI Cancer Center Support Grant (P30 CA142543).

* Fax: (+1)214-645-6370 jinming.gao@utsouthwestern.edu.

Supporting information for this article is available on the WWW under http://www.angewandte.org.

A. Dean Sherry, and
Advance Imaging Research Center, UT Southwestern Medical Center at Dallas, 5323 Harry Hines Blvds, Dallas.Texas 75390 (USA)

Jinming Gao*
Department of Pharmacology, Harold C. Simmons Comprehensive Cancer Center, UT Southwestern Medical Center at Dallas, 5323 Harry Hines Blvds, Dallas.Texas 75390 (USA)

Keywords

^{19}F MRI; pH responsive nanoprobe; barcode; pH imaging; activatable imaging agent

Magnetic resonance imaging (MRI) is a powerful noninvasive imaging technique that has greatly impacted basic biological research as well clinical diagnosis of cancer and other diseases.[1] Conventional MR contrast agents are T_1 (e.g. Gd-DTPA) or T_2-based (e.g. iron oxide), which cause significant longitudinal or transverse relaxation of protons, respectively.[2] Despite their success in many biological applications, one potential limitation is the lack of multi-chromatic features that allows for simultaneous detection of multiple signals. Recently, ^{19}F has received significant attention in MR imaging and spectroscopy studies.[3] Compared to ^{1}H-MRI, ^{19}F-MRI has little biological background due to the low levels of endogenous fluorine in the body. Moreover, ^{19}F has 100% natural abundance and its gyromagnetic ratio (40.06 MHz/T) is second only to ^{1}H, which makes it more sensitive for detection over other nuclei.[3f]

In this study, we report on the development of "multi-colored" pH-activatable ^{19}F-MRI nanoprobes with tunable pH transitions. Recently, extensive efforts have been dedicated to the development of stimuli-responsive nanoprobes.[4] Various nanosystems that respond to pH,[5] enzymatic expression,[6] redox reaction,[7] temperature,[8] and light[9] have been reported. Among these stimuli, pH stands out as an important physiological parameter that plays a critical role in both the intracellular (pH_i) and extracellular (pH_e) milieu.[10] For example, dysregulated pH was described as another hallmark of cancer, where a "reverse" pH gradient across the cell membrane is observed in cancer cells compared to normal cells.[11] A variety of different types of MRI agents have been reported for measuring pH,[12] but all have a rather broad pH response which may limit the accuracy of pH measurement, particularly when the pH perturbation in the pathological tissue is small. Moreover, it is often necessary to administer another pH-insensitive agent to correct for the contribution of agent concentration to obtain pH-sensitive signals, which makes the procedure complicated and difficult to perform.[13]

Herein we report the development of pH-sensitive ^{19}F-MRI nanoprobes with a binary (ON/OFF) response to a specific, narrow pH transition (0.25 pH unit). We theorize that a collection of such nanoprobes where each pH transition is encoded with a specific ^{19}F signature will allow for a simple readout of environmental pH through an "activation barcode". To demonstrate this proof of concept, we synthesized three ^{19}F-MRI nanoprobes with different pH transitions and ^{19}F-reporters (Scheme 1). Through these nanoprobes, we show in phantom studies the feasibility of using either ^{19}F spectroscopy or imaging to discriminate the pH differences in the microenvironment (i.e. 7.4, 6.5, 5.5 and 4.5).

The initial challenge in designing a set of multi-colored pH-activatable ^{19}F-nanoprobes is two-fold: first is the availability of reporter molecules that can be distinguished by MRS/I. For this purpose, ^{19}F is highly advantageous over ^{1}H probes as many ^{19}F reporter molecules have diverse chemical shifts and narrow peak widths that can be easily differentiated. The second is to devise an activation mechanism in which the signal intensities of these ^{19}F

reporter molecules are highly responsive to the pH changes in the environment. In this regard, we adopted a strategy of using changes in spin-spin relaxations between the micelle and unimer states to turn ON/OFF ^{19}F signals in response to pH.[3e, 3i] ^{19}F reporters are introduced to the ionizable block (PR) of amphiphilic copolymers consisting of hydrophilic PEO segment and tertiary amine/ammonium segment (Scheme 1b). We hypothesize that at pH > pK_a, hydrophobic micelle assembly results in highly restricted chain motions and short spin-spin relaxation times ($T_2 \rightarrow 0$) to effectively broaden and eliminate the ^{19}F signals; at pH < pK_a, protonation of ammonium groups will result in micelle disassembly, conformational flexibility in dissociated polymer chains, and reappearance of the previous ^{19}F signal.

For initial development, we first synthesized poly-(ethylene oxide)-*b*-poly[2-(diisopropylamino) ethyl methacrylate-*r*-trifluoroethyl methacrylate] (PEO-*b*-P(DPA-*r*-TFE)) copolymer using atom transfer radical polymerization method.[14] To investigate the optimal composition, we synthesized a series of PEO-*b*-P(DPA-*r*-TFE) copolymers with increasing molar ratios (5 to 75 mol%) of TFE component (Table S1-S2, Fig. S1). On one hand, a higher TFE content should lead to stronger ^{19}F signals while, too much TFE may override the pH response from DPA segment and induce micelle aggregation even at low pH. Gel permeation chromatography (GPC) and ^{1}H NMR characterization demonstrated that all copolymers had similar molecular weights (1.5-1.8 × 10^4 Da) and polydispersity (Table S1, Fig. S1). pH titration of the copolymers showed that the TFE content had a considerable influence on the pK_a and pH response of the copolymers. At 5 mol% of TFE, the pK_a is 6.3, similar to the PEO-*b*-PDPA copolymer without TFE.[5c] An increase in TFE content decreased the pK_a of the copolymers (Fig. S2a). Based on these pK_a values, we chose pH 4.0 (below the pK_a's of all the copolymers) to evaluate the effect of TFE content on ^{19}F signal intensity (δ_F = 2.3 ppm for TFE relative to TFA). The ^{19}F signal intensity as a funciton of TFE content showed a bell-shaped response curve, where it reached a maximum at 40 mol% TFE. At pH 4.0, dynamic light scattering experiments showed that all the copolymers except the PEO-*b*-P(DPA_{16}-*r*-TFE_{44}) (73 mol%) were in the unimer state as indicated by their small size (<10 nm in diameter) (Fig. S2c). Instead, PEO-*b*-P(DPA_{16}-*r*-TFE_{44}) copolymer formed micelles with a hydrodynamic diameter of 44 nm despite most of the amino groups were protonated at this pH. The decrease of ^{19}F intensity can be explained by the rapid increase of spin-spin relaxation (or decreased T_2) at higher molar fraction of TFE (Fig. S2e). Data show T_2 is relatively unchanged (>40 ms) when the TFE content is below 20 mol%. Based on these data, we chose 20 mol% (i.e. PEO-*b*-P(DPA_{48}-*r*-TFE_{12}) as the optimal ^{19}F-reporter composition in subsequent pH response studies.

^{19}F-NMR spectra of PEO-*b*-P(DPA_{48}-*r*-TFE_{12}) copolymer collected as a function of pH demonstrate ultra-pH responsive behavior (Fig. 1), similar to previously reported fluorescent nanoparticles.[5c, 5d] Below pH 6.0, we observed complete activation of ^{19}F signals; above pH 6.2, the ^{19}F signals largely disappeared. The pH difference ($\Delta pH_{10\text{-}90\%}$) between 10 to 90% signal difference is 0.25 pH. This ultra-pH response is a unique property of this class of ionizable amphiphilc block copolymers, where hydrophobicity-driven micellization dramatically increased the cooperative deprotonation of the ammonium blocks.[5c, 5d] Transmission electron microscopy (TEM) of PEO-*b*-P(DPA_{48}-*r*-TFE_{12}) verified the formation of micelles at pH 7.4 (above its pK_a of 6.1) and complete micelle dissociation at pH 5.0 (Fig. S3a). The micelle-unimer transition was further corroborated by ^{1}H NMR (Fig. S3b) and dynamic light scattering (DLS), where hydrodynamic diameters were changed from 40 to 6 nm at pH 7.4 and 5.0, respectively (Fig. S3c).

To investigate the ON/OFF pH-activatable MR imaging capability of the nanoprobes, we prepared a sample with two concentric tubes where both tubes were filled with PEO-P(DPA_{48}-*r*-TFE_{12}) at 25 mg/mL but the pH of the inner and outer tubes were controlled at

5.0 and 7.4, respectively. Axial ^{1}H MRI images showed two compartments with similar signal intensities (left panel, Fig. 2a). In contrast, the corresponding ^{19}F MRI images showed an intense signal (ON) in the inner tube but no signal (OFF) in the outer tube (right panel, Fig. 2a). We quantified the signal intensity in different regions of interest (ROI) over the background noise (Fig. 2b). At 55 mins, the ^{19}F SNR reached 31-fold for the PEO-*b*-P(DPA_{48}-*r*-TFE_{12}) nanoprobes at pH 5.0 (ON state). Then we compared the contrast of ^{19}F images between the ON and OFF states at pH 5.0 and 7.4, respectively. The contrast ratio ($SNR_{pH5.0}/SNR_{pH7.4}$) is 27 fold based on ^{19}F images, demonstrating that ^{19}F reporter on the polymers are highly responsive to the pH changes in the environment. In comparison, the $SNR_{pH5.0}/SNR_{pH7.4}$ ratio from the ^{1}H images was only 1.2.

Finally, we investigated the “barcode” concept using a mixture of ^{19}F-MRI nanoprobes with different pH transitions and ^{19}F reporter molecules to distinguish pH in the microenvironment. In addition to TFE (δ_F = 2.3 ppm), we introduced two additional ^{19}F reporter molecules (Scheme 1b, DFB and BTFB, δ_F = −33.2 and 13.0 ppm, respectively). These reporter molecules were incorporated into two new copolymers with different pH sensitivities, poly(ethylene oxide)-*b*-poly[2-(pentamethylene imino) methacrylate-*r*-2-(methacryloyloxy) ethyl 3,5-bis(trifluoromethyl) benzoate] (PEO-*b*-P(C6A-*r*-BTFB)) and poly(ethylene oxide)-*b*-poly[2-(dibutylamino) methacrylate-*r*-2-(methacryloyloxy) ethyl 3,5-difluorobenzoate] (PEO-*b*-P(DBA-*r*-DFB)) (Table S3). pH titration experiments demonstrated similar ultra-pH responsive properties of the two new copolymers (Fig. S4). The pK_a's of the PEO-*b*-P(C6A-*r*-BTFB) and PEO-*b*-P(DBA-*r*-DFB) copolymers were 7.0 and 5.0, respectively, in addition to PEO-*b*-P(DPA-*r*-TFE) (pK_a = 6.1). Based on these pK_a's, we defined a three-digit barcode where each digit corresponds to one nanoprobe (with pK_a from low to high), and has a binary response (1 for ON, 0 for OFF). For better visual demonstration, we also assigned a single color to each nanoprobe for the ON state (black for the OFF state). Such a barcode design allows for the direct readout of microenvionment pH within two adjacent pK_a's in which one nanoprobe is ON and the other is OFF (Fig. 3a).

To validate this concept, we performed a double blind experiment, where four solutions at pH 7.4, 6.5, 5.5 and 4.5 were first prepared containing the same mixture of the three nanoprobes. ^{19}F spectroscopy was then obtained for each solution. Figure 3b shows a clearly distinguished barcode pattern of nanoprobe activation. More specifically, the (000) solution corresponds to the solution at pH 7.4, where all the nanoprobes were OFF. Accordingly, the (001), (011) and (111) solutions correspond to solutions with pH values at 6.5, 5.5 and 4.5, respectively. The nanoprobe barcodes successfully distinguished the solution pH. Lastly, addition of fetal bovine serum (5 or 10%) in nanoprobe solutions at pH 4.5 did not affect the signal contrast significantly, demonstrating successful ^{19}F detection in biologically relevant media (Fig. S5).

In addition to ^{19}F spectroscopy, we also used ^{19}F MRI to spatially resolve the nanoprobe activation map. A phantom sample was prepared where 4 smaller tubes (each containing the same nanoprobe mixture in solutions at pH 7.4, 6.5, 5.5, and 4.5) were placed in a bigger tube with water only. T_1-weighted ^{1}H MRI images show similar signal intensity from all the tubes and the surrounding water (Fig. 3c). For ^{19}F MR imaging, we selectively activated each ^{19}F reporter at its chemical shift to examine the nanoprobe activation. Based on results from each ^{19}F channel, we were able to obtain the barcode information for the different regions of interest (Fig. 3c). Potentially, by combining the ^{19}F spectroscopy and imaging capabilities, we can generate a pH map where each voxel can be encoded with an activation barcode to indicate its environmental pH with spatial discrimination.

In summary, we report the feasibility of a series of multichromatic pH-activatable ^{19}F nanoprobes encoded with different ^{19}F reporters at specific pH transitions. Compared to

small molecular pH sensors (typically 2 pH unit for 10 fold signal change across pK_a), the pH response of these nanoprobes is extremely sharp ($\Delta pH_{ON/OFF}$~0.25 pH) and can be used as binary indicators for a specific pH transition. The current three nanoprobe collection provides the proof of concept and allows for a qualitative measurement of environmental pH. This nanoplatform can potentially overcome the instrument complexity and short T_1 limitation of the ^{13}C-based hyperpolarization probes.[15] Moreover, compared to chemical exchange saturation transfer (CEST) or ^{1}H agents where small pH-dependent chemical shifts are quantified,[12c, 16] the chemical shifts of ^{19}F reporters are widely separated and easily differentiated for binary readout and data processing. Development of additional nanoprobes with more refined pH transitions will be useful to narrow the pH transitions and improve the precision of pH measurement. In addition, use of hybrid nanoparticles to include all ^{19}F-encoded polymers in one system could further unify pharmacokinetics and biodistribution during *in vivo* study. Through a barcode map from ^{19}F-imaging spectroscopy, it is conceivable to generate a pH map in three dimensions. Along with these exciting potentials, one main challenge in subsequent preclinical translation of these nanoprobes is the relatively low detection sensitivity of ^{19}F-MRS/I. Optimization of MR scan time, pulse sequence or coil design should further improve the current detection limit (0.16 mg/mL ^{19}F). Image resolution can also be compromised to achieve higher detection sensitivity. Upon successful demonstration, the ^{19}F nanoprobes will add to the existing arsenal of pH sensors to measure tissue pH, an important physiological parameter in many pathological indications (e.g. cancer, inflammation, and osteoporosis).

Supplementary Material

Refer to Web version on PubMed Central for supplementary material.

References

1. a Caravan P, Ellison JJ, McMurry TJ, Lauffer RB. Chem. Rev. 1999; 99:2293–2352. [PubMed: 11749483] b Laurent S, Forge D, Port M, Roch A, Robic C, Vander Elst L, Muller RN. Chem. Rev. 2008; 108:2064–2110. [PubMed: 18543879] c Orel SG, Schnall MD. Radiology. 2001; 220:13–30. [PubMed: 11425968]
2. a Jun YW, Lee JH, Cheon J. Angew. Chem. Int. Ed. Engl. 2008; 47:5122–5135. [PubMed: 18574805] b Khemtong C, Kessinger CW, Gao J. Chem Commun (Camb). 2009:3497–3510. [PubMed: 19521593] c Sun C, Lee JS, Zhang M. Adv. Drug Delivery Rev. 2008; 60:1252–1265.
3. a Janjic JM, Srinivas M, Kadayakkara DK, Ahrens ET. J. Am. Chem. Soc. 2008; 130:2832–2841. [PubMed: 18266363] b Jiang ZX, Liu X, Jeong EK, Yu YB. Angew. Chem. Int. Ed. Engl. 2009; 48:4755–4758. [PubMed: 19475598] c Mizukami S, Takikawa R, Sugihara F, Hori Y, Tochio H, Walchli M, Shirakawa M, Kikuchi K. J. Am. Chem. Soc. 2008; 130:794–795. [PubMed: 18154336] d Mizukami S, Takikawa R, Sugihara F, Shirakawa M, Kikuchi K. Angew. Chem. Int. Ed. Engl. 2009; 48:3641–3643. [PubMed: 19353604] e Oishi M, Sumitani S, Nagasaki Y. Bioconjugate Chem. 2007; 18:1379–1382.f Ruiz-Cabello J, Barnett BP, Bottomley PA, Bulte JW. NMR Biomed. 2011; 24:114–129. [PubMed: 20842758] g Tanaka K, Kitamura N, Naka K, Chujo Y. Chem Commun (Camb). 2008:6176–6178. [PubMed: 19082111] h Yamaguchi K, Ueki R, Nonaka H, Sugihara F, Matsuda T, Sando S. J. Am. Chem. Soc. 2011; 133:14208–14211. [PubMed: 21851116] i Takaoka Y, Sakamoto T, Tsukiji S, Narazaki M, Matsuda T, Tochio H, Shirakawa M, Hamachi I. Nat. Chem. 2009; 1:557–561. [PubMed: 21378937] j Yu, JX.; Hallac, RR.; Chiguru, S.; Mason, RP. Prog. Nucl. Magn. Reson. Spectrosc. 2013. http://dx.doi.org/10.1016/j.pnmrs.2012.1010.1001k Yu JX, Kodibagkar VD, Cui W, Mason RP. Curr. Med. Chem. 2005; 12:819–848. [PubMed: 15853714]
4. a Lee ES, Gao Z, Bae YH. J. Controlled Release. 2008; 132:164–170.b Torchilin V. Eur. J. Pharm. Biopharm. 2009; 71:431–444. [PubMed: 18977297]
5. a Bae Y, Fukushima S, Harada A, Kataoka K. Angew. Chem. Int. Ed. Engl. 2003; 42:4640–4643. [PubMed: 14533151] b Lynn DM, Amiji MM, Langer R. Angew. Chem. Int. Ed. Engl. 2001;

40:1707–1710. [PubMed: 11353487] c Zhou K, Liu H, Zhang S, Huang X, Wang Y, Huang G, Sumer BD, Gao J. J. Am. Chem. Soc. 2012; 134:7803–7811. [PubMed: 22524413] d Zhou K, Wang Y, Huang X, Luby-Phelps K, Sumer BD, Gao J. Angew. Chem. Int. Ed. Engl. 2011; 50:6109–6114. [PubMed: 21495146] e Lee ES, Na K, Bae YH. J. Controlled Release. 2003; 91:103–113.

6. a Bernardos A, Aznar E, Marcos MD, Martinez-Manez R, Sancenon F, Soto J, Barat JM, Amoros P. Angew. Chem. Int. Ed. Engl. 2009; 48:5884–5887. [PubMed: 19575431] b Olson ES, Jiang T, Aguilera TA, Nguyen QT, Ellies LG, Scadeng M, Tsien RY. Proc. Natl. Acad. Sci. U. S. A. 2010; 107:4311–4316. [PubMed: 20160077] c Wang C, Chen Q, Wang Z, Zhang X. Angew. Chem. Int. Ed. Engl. 2010; 49:8612–8615. [PubMed: 20886493]
7. a Li YL, Zhu L, Liu Z, Cheng R, Meng F, Cui JH, Ji SJ, Zhong Z. Angew. Chem. Int. Ed. Engl. 2009; 48:9914–9918. [PubMed: 19937876] b Saito G, Swanson JA, Lee KD. Adv. Drug Delivery Rev. 2003; 55:199–215.
8. a Choi SW, Zhang Y, Xia Y. Angew. Chem. Int. Ed. Engl. 2010; 49:7904–7908. [PubMed: 20839209] b Jeong B, Bae YH, Kim SW. J. Controlled Release. 2000; 63:155–163.
9. a Skirtach AG, Munoz Javier A, Kreft O, Kohler K, Piera Alberola A, Mohwald H, Parak WJ, Sukhorukov GB. Angew. Chem. Int. Ed. Engl. 2006; 45:4612–4617. [PubMed: 16791887] b Volodkin DV, Skirtach AG, Mohwald H. Angew. Chem. Int. Ed. Engl. 2009; 48:1807–1809. [PubMed: 19173270] c Febvay S, Marini DM, Belcher AM, Clapham DE. Nano Lett. 2010; 10:2211–2219. [PubMed: 20446663]
10. Alberts, B.; Johnson, A.; Lewis, J.; Raff, M.; Roberts, K.; Walter, P. Molecular Biology of the Cell. 5th ed.. Garland Science; New York: 2008.
11. Webb BA, Chimenti M, Jacobson MP, Barber DL. Nat. Rev. Cancer. 2011; 11:671–677. [PubMed: 21833026]
12. a Aime S, Delli Castelli D, Terreno E. Angew. Chem. Int. Ed. Engl. 2002; 41:4334–4336. [PubMed: 12434381] b Gillies RJ, Raghunand N, Karczmar GS, Bhujwalla ZM. J. Magn. Reson. Imaging. 2002; 16:430–450. [PubMed: 12353258] c Sheth VR, Li Y, Chen LQ, Howison CM, Flask CA, Pagel MD. Magn. Reson. Med. 2012; 67:760–768. [PubMed: 22028287] d Ward KM, Balaban RS. Magn. Reson. Med. 2000; 44:799–802. [PubMed: 11064415] e Zhou J, Payen JF, Wilson DA, Traystman RJ, van Zijl PC. Nat. Med. 2003; 9:1085–1090. [PubMed: 12872167] f Zhang S, Wu K, Sherry AD. Angew. Chem. Int. Ed. Engl. 1999; 38:3192–3194. [PubMed: 10556899] g Wu Y, Soesbe TC, Kiefer GE, Zhao P, Sherry AD. J. Am. Chem. Soc. 2010; 132:14002–14003. [PubMed: 20853833]
13. a Garcia-Martin ML, Martinez GV, Raghunand N, Sherry AD, Zhang S, Gillies RJ. Magn. Reson. Med. 2006; 55:309–315. [PubMed: 16402385] b Raghunand N, Howison C, Sherry AD, Zhang S, Gillies RJ. Magn. Reson. Med. 2003; 49:249–257. [PubMed: 12541244]
14. a Tsarevsky NV, Matyjaszewski K. Chem. Rev. 2007; 107:2270–2299. [PubMed: 17530906] b Ma YH, Tang YQ, Billingham NC, Armes SP, Lewis AL, Lloyd AW, Salvage JP. Macromolecules. 2003; 36:3475–3484.
15. Gallagher FA, Kettunen MI, Day SE, Hu DE, Ardenkjaer-Larsen JH, Zandt R, Jensen PR, Karlsson M, Golman K, Lerche MH, Brindle KM. Nature. 2008; 453:940–943. [PubMed: 18509335]
16. a Provent P, Benito M, Hiba B, Farion R, Lopez-Larrubia P, Ballesteros P, Remy C, Segebarth C, Cerdan S, Coles JA, Garcia-Martin ML. Cancer Res. 2007; 67:7638–7645. [PubMed: 17699768] b McMahon MT, Gilad AA, DeLiso MA, Berman SM, Bulte JW, van Zijl PC. Magn. Reson. Med. 2008; 60:803–812. [PubMed: 18816830]

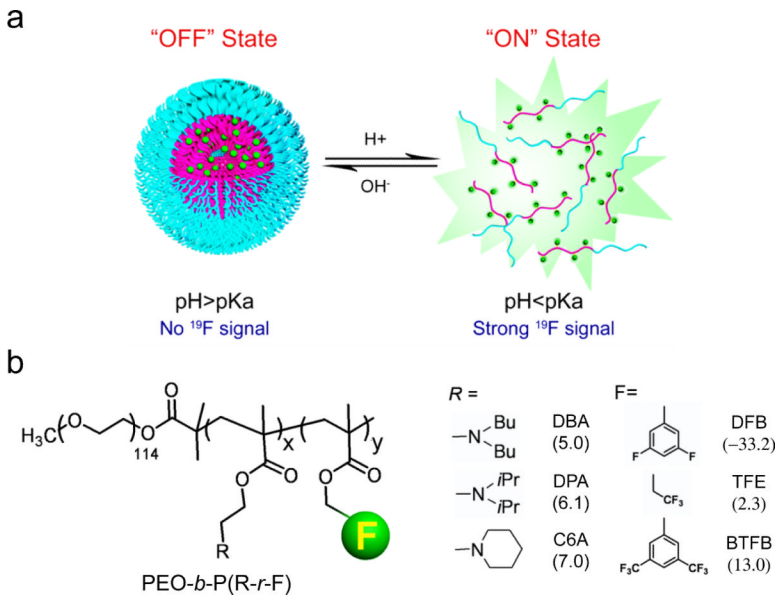

Scheme 1.

(a) Schematic of pH-activatable ON/OFF ^{19}F-MRI nanoprobes from ionizable diblock copolymers. At pH > pK_a, the hydrophobic segments self-assemble into micelle core leading to ^{19}F signal suppression due to restricted polymer chain motion. Upon pH activation (pH < pK_a), micelle disassembly leads to dissociated unimers and strong ^{19}F signal. (b) Chemical structures of three representative diblock copolymers containing different pH responsive segments and ^{19}F reporter moieties, where their pK_a's and ^{19}F chemical shifts (in ppm, relative to trifluoroacetic acid, or TFA) are shown in parenthesis, respectively.

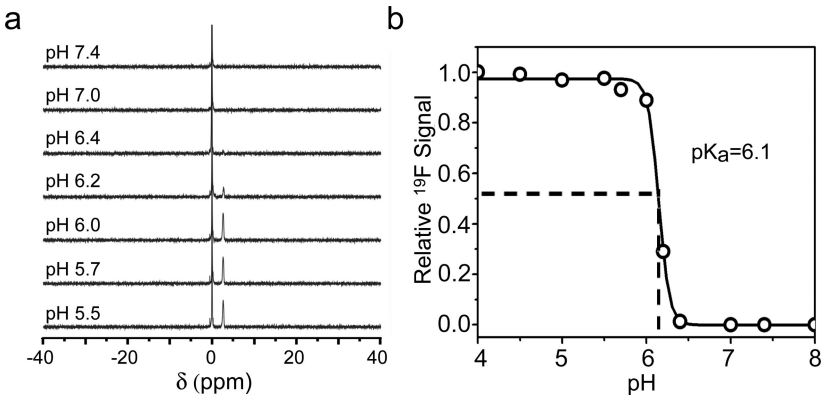

Figure 1.

(a) ^{19}F spectra of 2 mg/mL PEO-*b*-P(DPA_{48}-*r*-TFE_{12}) micelles in deuterated acetate buffers at different pH. TFA was used as an external reference with its chemical shift set as 0. (b) Normalized ^{19}F signal intensity as a function of pH. Data was obtained from (a).

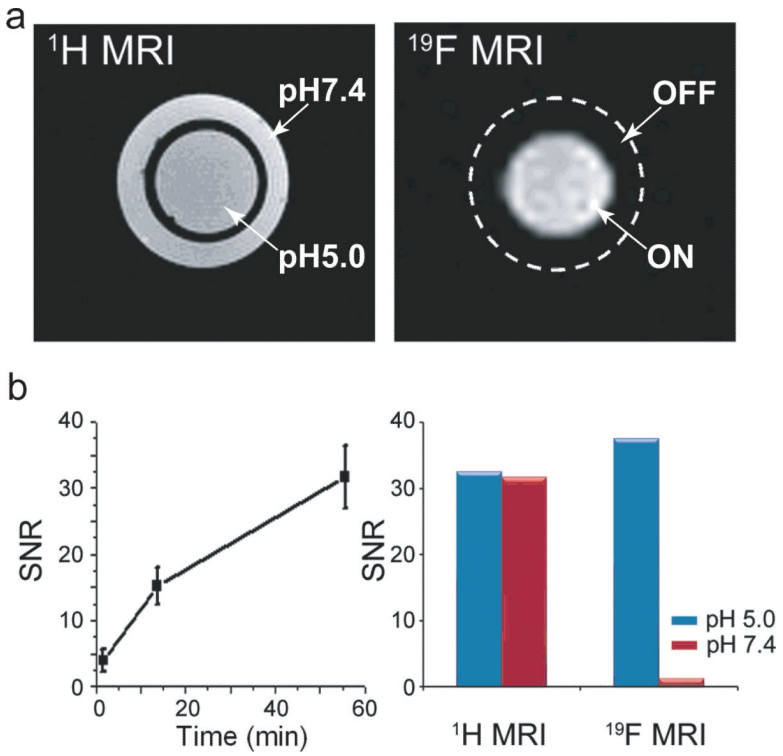

Figure 2.

(a) ^{1}H and ^{19}F MRI images of PEO-*b*-P(DPA$_{48}$-*r*-TFE$_{12}$) (25 mg/mL) phantom at pH 5.0 (inner tube) and 7.4 (outer tube). (b) SNR of ^{19}F signals for PEO-*b*-P(DPA$_{48}$-*r*-TFE$_{12}$) as a function of scanning time at pH 5.0 (left panel) and comparison of SNR ratios at pH 5.0 and 7.4 from both ^{1}H and ^{19}F MRI images (right).

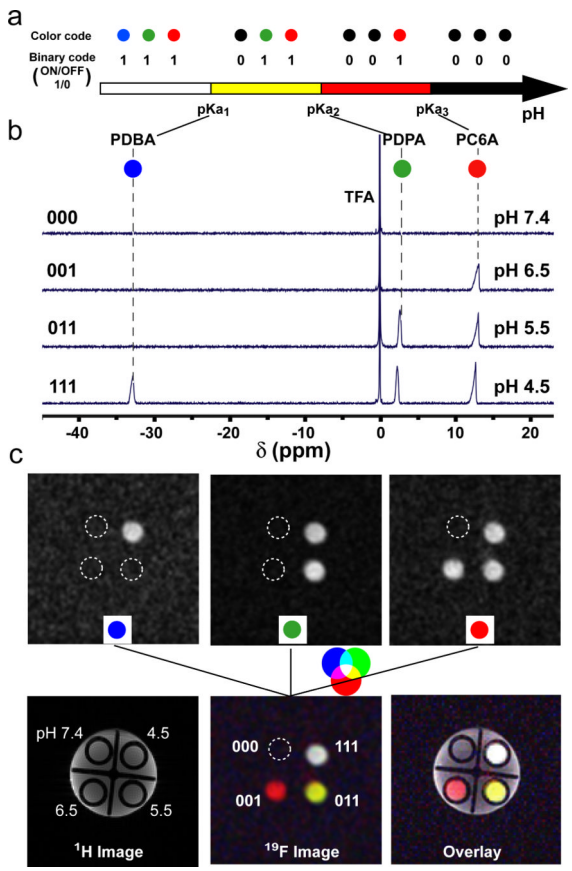

Figure 3.

(a) Schematic illustration of the activation barcode concept for direct readout of pH within adjacent pK_a's. See text for details. (b) ^{19}F spectra of a mixture of three PEO-*b*-P(R-*r*-F) nanoprobes in acetate buffers of different pH (7.4, 6.5, 5.5, 4.5). TFA was used as an external reference. (c) ^{19}F MR imaging of the same nanoprobe mixture in solutions with different pH. Detection of each ^{19}F reporter was accomplished by selective activation at its chemical shift (upper three panels). A “barcode map” (bottom middle panel) can be obtained by fusion of three ^{19}F reporter images. ^{19}F MR image was overlayed with ^{1}H image to show the spatial registration.